Quaternary fission in $^{244–254}$Cf isotopes with two α particles as middle fragments

K. P. Santhosh* and Annu Cyriac
School of Pure and Applied Physics, Kannur University, Swami Anandatheertha Campus, Payyanur 670327, Kerala, India

(Received 6 January 2020; accepted 18 February 2020; published 20 April 2020)

The quaternary fission of $^{244–254}$Cf isotope with two α particles as the middle fragments in collinear configuration has been studied by taking the interacting barrier as the sum of Coulomb and nuclear proximity potential. The most favorable quaternary fission path is the one that has a high Q value and a minimum driving potential with respect to the mass and charge asymmetries. The favorable fragment combinations are obtained from the cold reaction valley plot and then calculating the yield for charge minimized fragments. For ^{244,248,254}Cf isotopes, the highest yield is predicted for the isotope of Sb as one fragment, ^{134}Sb ($Z = 51$, $N = 83$), ^{130}Sb ($Z = 51$, $N = 79$), ^{132}Sb ($Z = 51$, $N = 81$), respectively, whereas for ^{246}Cf isotope, fragments with isotope of I as one fragment ^{134}I ($Z = 53$, $N = 81$) possesses the highest yield. For ^{250}Cf isotope, fragments with isotope of In as one fragment, ^{132}In ($Z = 49$, $N = 83$) possesses the highest yield. In the case of ^{252}Cf isotope, the highest yield is for the fragments with Te as one fragment, ^{132}Te ($Z = 52$, $N = 80$). These findings confirm the role of doubly magic or near doubly magic nucleus in quaternary fission, which supports the conclusion by Poenaru *et al.* [Nucl. Phys. A **747**, 182 (2005)]. The deformation and orientation of fragments has also been taken into account for the two α accompanied quaternary fission, and it has been found that in addition to closed shell effect, ground-state deformation also plays an important role in determining the isotopic yield in the quaternary fission process. We hope that our study on isotopic yield in quaternary fission of even-even $^{244–254}$Cf isotope will be a guide for future experiments.

DOI: 10.1103/PhysRevC.101.044613

I. INTRODUCTION

Usually fission of actinide nuclei proceeds by decay into two fragments of comparable size. With probabilities at the level of 10^{-3} per binary fission, a third, in most cases light charged particle (LCP), accompanies the customary fission fragments. The process is called ternary fission (TF). There is ample evidence from experimental studies and also from the theoretical point of view that the majority of light charged particles are born right at the scission in the neck region of the nascent fission fragments. A generalization of ternary fission process, where there is a possibility for two light charged particles formed along with the two main fission fragments, can be termed as a quaternary fission. The theoretical studies on the basis of quaternary fission has been found to be noteworthy, as this type of decay process takes place with probabilities of 10^{-7} per binary fission. Due to this low probability level, the quaternary fission has been barely studied in the past. In most of the quaternary fission process, the α particles and H isotopes (mostly tritium) are found to be the favorable light charged particles. The quaternary fission process takes place in two possible modes, the simultaneous or true quaternary and sequential or pseudoquaternary decays. In true quaternary fission, the fission fragments are formed almost simultaneously in the vicinity of nucleus scission point. The pseudoquaternary fission is a sequential decay process and takes place in two stages. The first stage is a ternary fission process with the emission of an unstable light particle, which decays into two light charged particles as the second stage of the fission mechanism. For example, the unstable light nuclei ^{8}Be, in the ground or excited state, formed in the ternary fission process as the first stage decays into two α particles in the second stage. The true quaternary and pseudoquaternary fission process can be distinguished by inspecting the angular correlations between the two outgoing light charged particles. The first pieces of experimental evidence of the existence of quaternary nuclear fission were obtained in studying the reaction ^{235}U(n, f) induced by thermal neutrons [1] and in studying the spontaneous fission of ^{248}Cm [2] nucleus. More detailed investigations of quaternary fission were performed in Ref. [3] for the fission of ^{233}U and ^{235}U nuclei that was induced by cold neutrons, and in for the spontaneous fission of ^{252}Cf. In those studies, the yields and angular energy distributions were analyzed for pairs of light third and fourth particles produced with the highest probability such as (α, α), (α, t), and (t, t).

In this paper, a systematic and detailed study on the isotopic yield of quaternary fission of $^{244–254}$Cf isotopes was carried out for the first time by taking the interacting barrier as the sum of Coulomb and nuclear proximity potential. Mutterer *et al.*, [4] experimentally observed that in quaternary fission of ^{252}Cf, two α particles are emitted as the light charged particle. Hence in our study we have considered two α particles as the middle fragment, which revealed the new aspects of the process of particle-accompanied fission. The light charged

*drkpsanthosh@gmail.com

particles are born right at scission in the neck region between the two nascent fission fragments. We would like to mention that by taking the interacting barrier as the sum of Coulomb and nuclear proximity potential, the binary fission of $^{244–258}$Cf isotopes and $^{238–248}$Pu isotopes has been studied by Santhosh *et al.*, [5,6] where the cold reaction valleys are plotted and the corresponding barrier penetrability and yields are calculated for all binary fragmentations of the above-mentioned isotopes.

The methodology employed for our calculation is described in Sec. II. The details of the study can be found in Sec. III, results and discussion. Conclusions are summarized in Sec. IV.

II. MODEL

Two light charged particle accompanied quaternary fission is energetically possible only if the Q value of the reaction is positive. i.e.,

$$Q = M - \sum_{i=1}^{4} m_i > 0. \tag{1}$$

Here M is the mass excess of the parent, m_i is the mass excess of the fragments. The interacting potential barrier for a parent nucleus exhibiting cold quaternary fission consists of Coulomb potential and nuclear proximity potential of Blocki *et al.*, [7] and is given by

$$V = \sum_{i=1}^{4} \sum_{j>i}^{4} (V_{Cij} + V_{Pij}) \tag{2}$$

with $V_{Cij} = \frac{Z_i Z_j e^2}{r_{ij}}$, the Coulomb interaction between the fragments. Here Z_i and Z_j are the atomic numbers of the fragments and r_{ij} is the distance between fragment centers. The nuclear proximity potential between the fragments is

$$V_{Pij}(z) = 4\pi\gamma b \left[\frac{C_i C_j}{C_i + C_j}\right] \Phi\left(\frac{z}{b}\right). \tag{3}$$

Here $z = z_{12} = z_{23} = z_{34}$ is the distance between the near surfaces of the fragments. The nuclear surface tension coefficient γ is given by,

$$\gamma = 0.9517[1 - 1.7826(N - Z)^2/A^2]\,\mathrm{MeV/fm^2}, \tag{4}$$

where N, Z, and A represents neutron, proton, and mass number of parent, respectively, Φ represents the universal proximity potential [8] given as,

$$\Phi(\xi) = -4.41e^{-\xi/0.7176} \quad \text{for } \xi > 1.9475, \tag{5}$$

$$\Phi(\xi) = -1.7817 + 0.9270\xi + 0.0169\xi^2 - 0.05148\xi^3 \quad \text{for } 0 \leqslant \xi \leqslant 1.9475 \tag{6}$$

with $\xi = z/b$, where the width (diffuseness) of the nuclear surface $b \approx 1$ fm and Süsmann central radii C_i of fragments related to sharp radii R_i as,

$$C_i = R_i - \left(\frac{b^2}{R_i}\right). \tag{7}$$

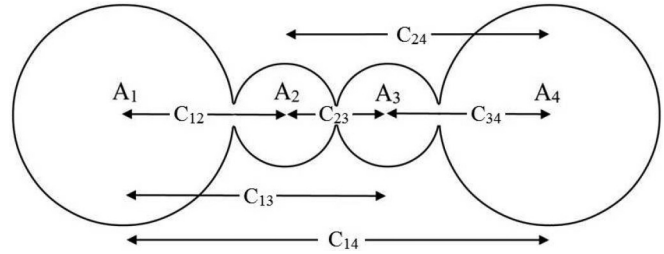

FIG. 1. The touching configuration of four spherical fragments in the case of quaternary fission.

For R_i we use semiempirical formula in terms of mass number A_i as [7],

$$R_i = 1.28A_i^{1/3} - 0.76 + 0.8A_i^{-1/3}. \tag{8}$$

Using one-dimensional WKB approximation, the barrier penetrability P is given as,

$$P = \exp\left\{-\frac{2}{\hbar}\int_{z_1}^{z_2} \sqrt{2\mu(V - Q)}dz\right\}. \tag{9}$$

The turning points $z_1 = 0$ represents the touching configuration and outer turning point z_2 is determined from the equation $V(z_2) = Q$, where Q is the decay energy. The potential V in Eq. (9), which is the sum of Coulomb and proximity potential given by Eq. (2), is computed by varying the distance between the near surfaces of the fragments. Here the reduced mass μ is expressed as,

$$\mu = m\left(\frac{A_1A_2A_3A_4}{A_2A_3A_4 + A_1A_3A_4 + A_1A_2A_4 + A_1A_2A_3}\right), \tag{10}$$

where m is the nucleon mass and A_1, A_2, A_3, A_4 are the mass numbers of the four fragments. The ratio between the penetration probabilities of a given fragmentation over the sum of penetration probabilities of all possible fragmentation is calculated as the relative yield and is given as,

$$Y(A_i, Z_i) = \frac{P(A_i, Z_i)}{\sum P(A_i, Z_i)}. \tag{11}$$

III. RESULTS AND DISCUSSION

The quaternary fragmentation of $^{244–254}$Cf isotopes with two α particles as the middle fragments in collinear configuration is studied using the concept of cold reaction valley, which was introduced in relation to the structure of minima in the so-called driving potential. The driving potential is the difference between the interaction potential, V and the decay energy, Q of the reaction. The interaction potential is taken as the sum of Coulomb and nuclear proximity potential. The barrier penetrability is very sensitive to the Q value and is computed using the standard mass tabulated in Refs. [9,10] for the mass of parent and fragments. Figure 1 represents the schematic representation of collinear configuration of four fragments at the touching configuration.

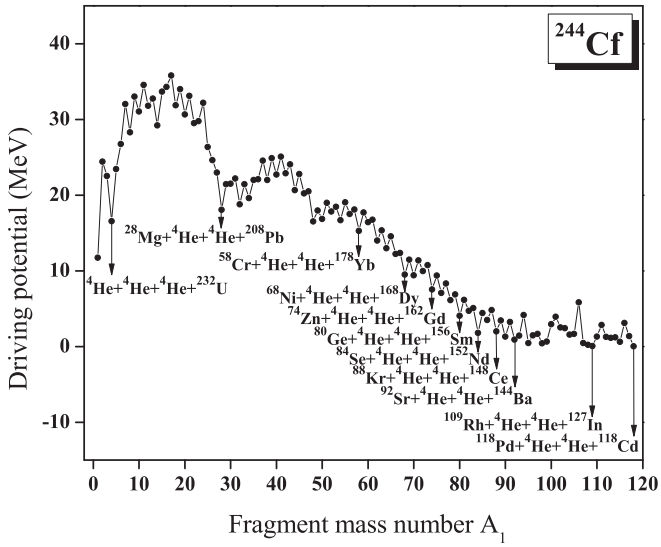

FIG. 2. The driving potential for ^{244}Cf isotope with emission of two α particles as light charged particle, plotted as a function of mass number A_1.

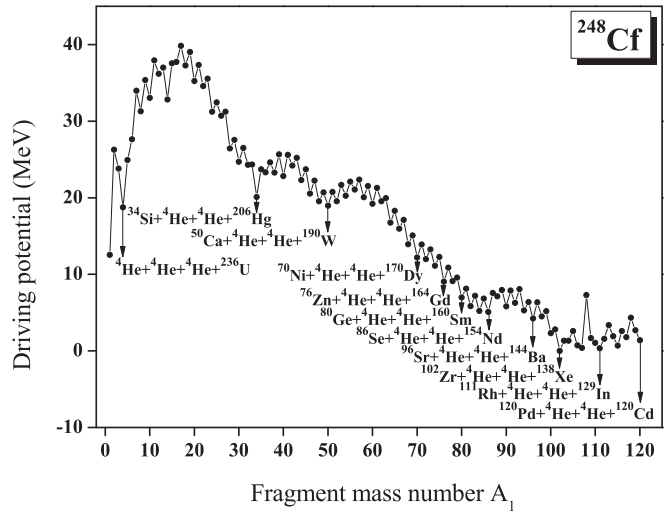

FIG. 4. The driving potential for ^{248}Cf isotope with emission of two α particles as light charged particle, plotted as a function of mass number A_1.

A. Cold reaction valley of even-even $^{244-254}$Cf isotopes

In the case of quaternary fission of $^{244-254}$Cf isotopes, its driving potential for the touching configuration ($z = 0$) of fragment combinations are calculated. Figures 2–7 represent the plots for driving potential versus A_1 (mass of one fragment) for all the above isotopes. Observed mass-asymmetry valleys in these figures are because of the shell effects of one or both the fragments. The fragment combinations having minima in the potential energy are the most probable quaternary fission fragments.

For ^{244}Cf, a deep minimum is observed at $^{118}\text{Pd} + {}^{4}\text{He} + {}^{4}\text{He} + {}^{118}\text{Cd}$ due to the near proton shell closure $Z = 48$ of ^{118}Cd whereas for ^{246}Cf it is seen for the fragment configuration $^{102}\text{Nb} + {}^{4}\text{He} + {}^{4}\text{He} + {}^{136}\text{I}$ due to the near doubly magic nucleus ^{136}I ($N = 83$, $Z = 53$). In the case of ^{248}Cf deepest minimum is for the fragment configuration $^{102}\text{Zr} + {}^{4}\text{He} + {}^{4}\text{He} + {}^{138}\text{Xe}$ due to the near doubly magic nucleus ^{138}Xe ($N = 84$, $Z = 54$). For ^{250}Cf, the deepest minimum is found for the fragment configuration $^{103}\text{Nb} + {}^{4}\text{He} + {}^{4}\text{He} + {}^{139}\text{I}$ due to the near doubly magic nucleus ^{139}I ($N = 86$, $Z = 53$) whereas for ^{252}Cf it is seen for the fragment configuration $^{113}\text{Tc} + {}^{4}\text{He} + {}^{4}\text{He} + {}^{131}\text{Sb}$, and is due to the near doubly magic nucleus ^{131}Sb ($N = 80$, $Z = 51$). In the case of ^{254}Cf deepest minimum is for the

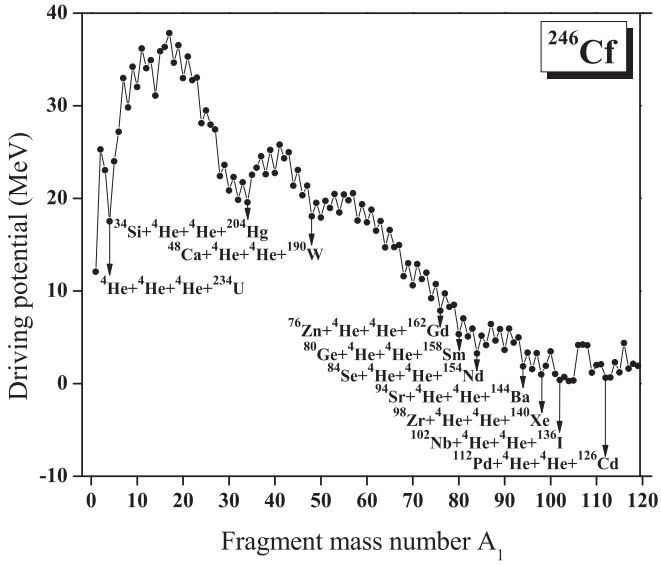

FIG. 3. The driving potential for ^{246}Cf isotope with emission of two α particles as light charged particle, plotted as a function of mass number A_1.

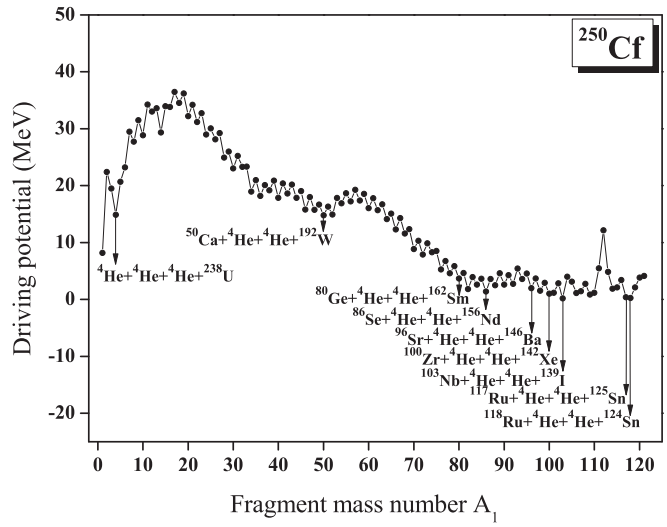

FIG. 5. The driving potential for ^{250}Cf isotope with emission of two α particles as light charged particle, plotted as a function of mass number A_1.

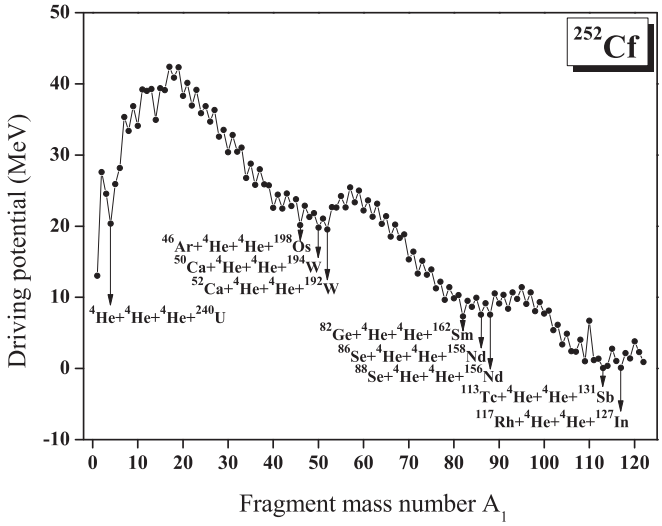

FIG. 6. The driving potential for ^{252}Cf isotope with emission of two α particles as light charged particle, plotted as a function of mass number A_1.

fragment configuration ^{112}Tc + ^{4}He + ^{4}He + ^{134}Sb, and is due to the near doubly magic nucleus ^{134}Sb ($N = 83$, $Z = 51$). The other minima observed are labeled in the corresponding figures.

B. Barrier penetrability and yield calculation

The barrier penetrability for each fragment combinations found in the cold valley for $^{244–254}$Cf isotopes are calculated. The most favorable fragment combinations for all the six isotopes mentioned above are obtained by calculating their relative yields. Using Eq. (11) relative yield is calculated and is plotted as a function of fragment mass number A_1 and A_2.

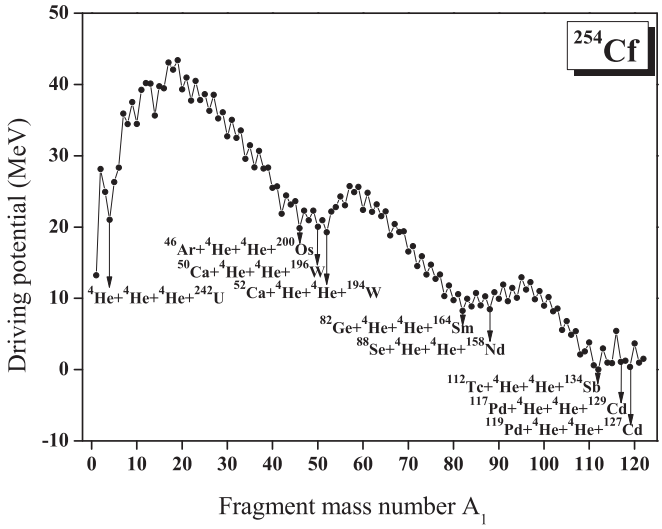

FIG. 7. The driving potential for ^{254}Cf isotope with emission of two α particles as light charged particle, plotted as a function of mass number A_1.

While analyzing the plot for ^{244}Cf, it is clear that the fragment combination ^{102}Tc + ^{4}He + ^{4}He + ^{134}Sb possess the highest yield due to the presence of near doubly magic nucleus ^{134}Sb ($Z = 51, N = 83$). The second highest yield is observed for the fragment combination ^{108}Mo + ^{4}He + ^{4}He + ^{128}Te due to the near proton shell closure $Z = 52$ of ^{128}Te. The other various peaks in the relative yield graph correspond to fragment combinations ^{104}Nb + ^{4}He + ^{4}He + ^{132}I and ^{106}Rh + ^{4}He + ^{4}He + ^{130}In. Among these combinations, the first one is attributed to the near proton shell closure $Z = 53$ of ^{132}I and the second combination is due to near doubly magic nucleus ^{130}In ($Z = 49, N = 81$).

For ^{246}Cf, highest maximum of the yield graph belongs to the fragment combination ^{104}Nb + ^{4}He + ^{4}He + ^{134}I. This favorable channel is due to the presence of near doubly magic nucleus ^{134}I ($Z = 53$, $N = 81$). The next peak of the relative yield graph comes from the fragment combination ^{108}Rh + ^{4}He + ^{4}He + ^{130}In due to the presence of near doubly magic nucleus ^{130}In ($Z = 49, N = 81$).

In the case of quaternary fission of ^{248}Cf isotopes with two α particles as the middle fragments, the highest maximum of the yield belongs to the fragment combination ^{110}Tc + ^{4}He + ^{4}He + ^{130}Sb due to the presence of near proton shell closure $Z = 51$ of ^{130}Sb.

For quaternary fission of ^{250}Cf isotopes with ^{4}He as the fixed second and third fragments, the highest maximum of the yield graph belongs to the fragment combination ^{110}Rh + ^{4}He + ^{4}He + ^{132}In due to the presence of near doubly magic nucleus ^{132}In ($Z = 49$, $N = 83$). The second highest yield is observed for the fragment combination ^{112}Nb + ^{4}He + ^{4}He + ^{130}I due to the near proton shell closure $Z = 53$ of ^{130}I.

For ^{252}Cf and ^{254}Cf isotopes, the fragment combination ^{112}Mo + ^{4}He + ^{4}He + ^{132}Te and ^{114}Tc + ^{4}He + ^{4}He + ^{132}Sb, respectively, possess the highest yield due to the presence of near doubly magic nucleus ^{132}Te ($Z = 52, N = 80$) and ^{132}Sb ($Z = 51, N = 81$).

C. Role of deformation and orientation of fragments

The effect of deformation and orientation of fragments in two α accompanied quaternary fission of even-even $^{244–254}$Cf isotopes have been analyzed taking the Coulomb and proximity potential as the interacting barrier. The Coulomb interaction between the two deformed and oriented nuclei, which is taken from Ref. [11] and which includes higher multipole deformation [12,13], is given as,

$$V_C = \frac{Z_1 Z_2 e^2}{r} + 3Z_1 Z_2 e^2 \sum_{\lambda,i=1,2} \frac{1}{2\lambda+1} \frac{R_{0i}^{\lambda}}{r^{\lambda+1}} Y_{\lambda}^{(0)}(\alpha_i) \times \left[\beta_{\lambda i} + \frac{4}{7}\beta_{\lambda i}^2 Y_{\lambda}^{(0)}(\alpha_i)\delta_{\lambda,2}\right] \quad (12)$$

with

$$R_i(\alpha_i) = R_{0i}\left[1 + \sum_{\lambda} \beta_{\lambda i} Y_{\lambda}^{(0)}(\alpha_i)\right], \quad (13)$$

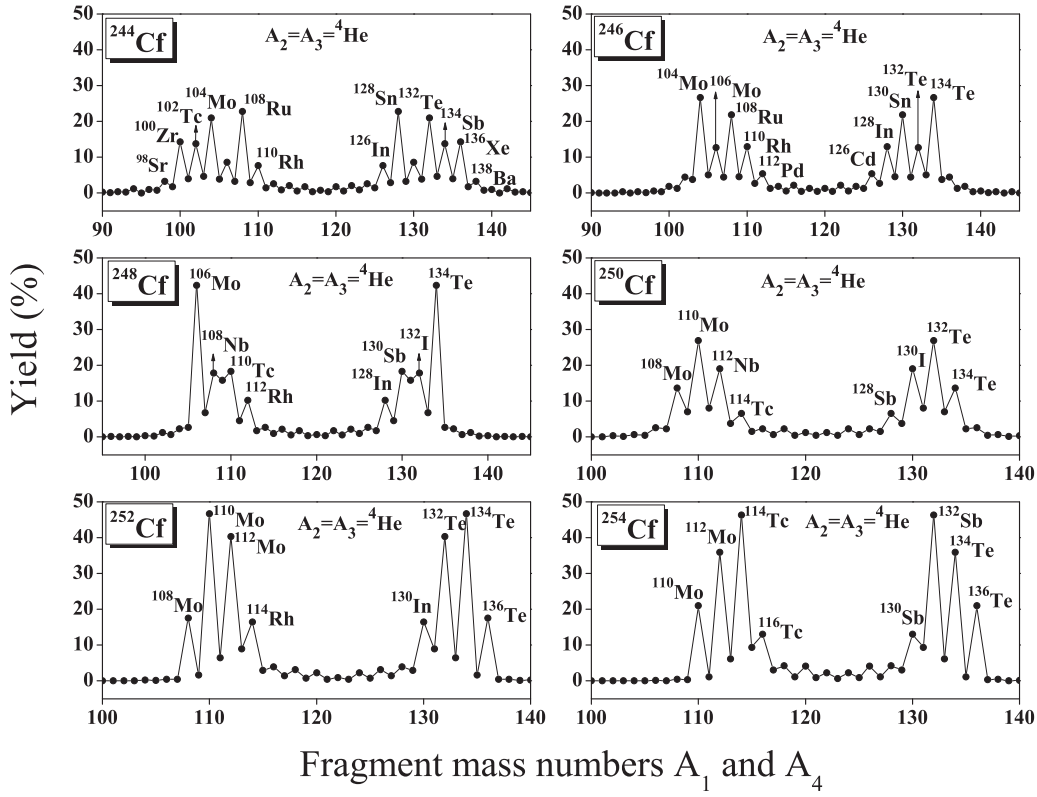

FIG. 8. The calculated yield for the quaternary fission of $^{244-254}$Cf isotopes plotted as a function of mass numbers A_1 and A_4, considering both deformation and orientation effects. The fragment combinations with higher yields are labeled.

where $R_{0i} = 1.28A_i^{1/3} - 0.76 + 0.8A_i^{-1/3}$. Here α_i is the angle between the radius vector and symmetry axis of the ith nuclei (see Fig. 1 of Ref. [12]) and it is to be noted that the quadrupole interaction term proportional to $\beta_{21}\beta_{22}$, is neglected because of its short-range character.

In proximity potential, $V_P(z) = 4\pi\gamma b\overline{R}\Phi(\varepsilon)$, the deformation comes only in the mean curvature radius. For spherical nuclei, mean curvature radius is defined as $\overline{R} = \frac{C_1C_2}{C_1+C_2}$ where C_1 and C_2 are Süssmann central radii of fragments. The mean curvature radius, $\overline{R}$ for two deformed nuclei lying in the same plane can be obtained by the relation,

$$\frac{1}{\overline{R}^2} = \frac{1}{R_{11}R_{12}} + \frac{1}{R_{21}R_{22}} + \frac{1}{R_{11}R_{22}} + \frac{1}{R_{21}R_{12}}. \qquad (14)$$

The four principal radii of curvature R_{11}, R_{12}, R_{21}, and R_{22} are given by Baltz and Bayman [14].

For computing driving potential, we have used experimental quadrupole deformation (β_2) values taken from Ref. [15] and for those cases where the experimental values were unavailable, we have taken them from Moller *et al.* [16]. It is observed that in most of the cases, 0°–0° orientation have a low value for driving potential, but in few cases, 90°–90° orientation has the low value. In the former case, either both the fragments are prolate or one fragment is prolate and the other one is spherical; and in latter case both fragments are either oblate or one fragment is oblate and the other one is spherical. It is observed that when deformation is included, the optimum fragment combinations in the cold valley are also found to be changed. For example, in the case of ^{244}Cf isotope, the fragment combinations ^{118}Pd + ^{4}He + ^{4}He + ^{118}Cd and ^{109}Rh + ^{4}He + ^{4}He + ^{127}In changed to ^{118}Rh + ^{4}He + ^{4}He + ^{118}In and ^{109}Ru + ^{4}He + ^{4}He + ^{127}Sn, respectively. In the case of ^{246}Cf isotope, the fragment combinations ^{102}Nb + ^{4}He + ^{4}He + ^{136}I and ^{112}Pd + ^{4}He + ^{4}He + ^{126}Cd changed to ^{102}Zr + ^{4}He + ^{4}He + ^{136}Xe and ^{112}Nb + ^{4}He + ^{4}He + ^{126}I, respectively. In the case of ^{248}Cf isotope, the fragment combinations ^{102}Zr + ^{4}He + ^{4}He + ^{138}Xe and ^{111}Rh + ^{4}He + ^{4}He + ^{129}In changed to ^{102}Nb + ^{4}He + ^{4}He + ^{138}I and ^{111}Mo + ^{4}He + ^{4}He + ^{129}Te, respectively. In the case of ^{250}Cf isotope, the fragment combinations ^{103}Nb + ^{4}He + ^{4}He + ^{139}I and ^{118}Ru + ^{4}He + ^{4}He + ^{124}Sn changed to ^{103}Zr + ^{4}He + ^{4}He + ^{139}Xe and ^{118}Rh + ^{4}He + ^{4}He + ^{124}In, respectively. In the case of ^{252}Cf isotope, the fragment combinations ^{113}Tc + ^{4}He + ^{4}He + ^{131}Sb and ^{117}Rh + ^{4}He + ^{4}He + ^{127}In changed to ^{113}Nb + ^{4}He + ^{4}He + ^{131}I and ^{117}In + ^{4}He + ^{4}He + ^{127}Rh, respectively. In the case of ^{254}Cf isotope, the fragment combinations ^{112}Tc + ^{4}He + ^{4}He + ^{134}Sb and ^{119}Pd + ^{4}He + ^{4}He + ^{127}Cd changed to ^{112}Mo + ^{4}He + ^{4}He + ^{134}Te and ^{119}In + ^{4}He + ^{4}He + ^{127}Rh, respectively.

By including the quadrupole deformation, the barrier penetrability is calculated for all possible fragment combinations that occur in the cold valley plot, which have the minimum ($V - Q$) value. The computations are done using the deformed Coulomb potential and deformed nuclear proximity potential. The inclusion of quadrupole deformation (β_2) reduces the

TABLE I. The Q values and yield for the most favorable fragment combinations for the quaternary fission of $^{244-254}$Cf isotopes.

Parent Nucleus	A_1	A_2	A_3	A_4	Q value (MeV)	Yield (%)
^{244}Cf	^{98}Sr	^{4}He	^{4}He	^{138}Ba	217.8	3.283
^{244}Cf	^{100}Zr	^{4}He	^{4}He	^{136}Xe	219.3	14.389
^{244}Cf	^{102}Tc	^{4}He	^{4}He	^{134}Sb	216.8	13.789
^{244}Cf	^{104}Mo	^{4}He	^{4}He	^{132}Te	222.0	20.982
^{244}Cf	^{108}Ru	^{4}He	^{4}He	^{128}Sn	223.5	22.806
^{244}Cf	^{110}Rh	^{4}He	^{4}He	^{126}In	217.2	7.626
^{246}Cf	^{104}Mo	^{4}He	^{4}He	^{134}Te	222.0	26.721
^{246}Cf	^{106}Mo	^{4}He	^{4}He	^{132}Te	220.4	12.697
^{246}Cf	^{108}Ru	^{4}He	^{4}He	^{130}Sn	222.9	21.813
^{246}Cf	^{110}Rh	^{4}He	^{4}He	^{128}In	216.2	12.972
^{246}Cf	^{112}Pd	^{4}He	^{4}He	^{126}Cd	217.8	5.408
^{248}Cf	^{106}Mo	^{4}He	^{4}He	^{134}Te	220.9	42.392
^{248}Cf	^{108}Nb	^{4}He	^{4}He	^{132}I	207.6	17.858
^{248}Cf	^{109}Ru	^{4}He	^{4}He	^{131}Sn	220.3	15.856
^{248}Cf	^{110}Tc	^{4}He	^{4}He	^{130}Sb	222.5	18.344
^{248}Cf	^{112}Rh	^{4}He	^{4}He	^{128}In	221.2	10.294
^{250}Cf	^{108}Mo	^{4}He	^{4}He	^{134}Te	219.5	13.646
^{250}Cf	^{110}Mo	^{4}He	^{4}He	^{132}Te	220.8	26.877
^{250}Cf	^{112}Nb	^{4}He	^{4}He	^{130}I	202.3	19.019
^{250}Cf	^{114}Tc	^{4}He	^{4}He	^{128}Sb	214.4	6.581
^{252}Cf	^{108}Mo	^{4}He	^{4}He	^{136}Te	216.2	17.516
^{252}Cf	^{112}Mo	^{4}He	^{4}He	^{132}Te	213.8	40.312
^{252}Cf	^{114}Rh	^{4}He	^{4}He	^{130}In	216.7	16.464
^{254}Cf	^{110}Mo	^{4}He	^{4}He	^{136}Te	215.3	21.021
^{254}Cf	^{112}Mo	^{4}He	^{4}He	^{134}Te	216.3	35.939
^{254}Cf	^{114}Tc	^{4}He	^{4}He	^{132}Sb	214.7	46.334
^{254}Cf	^{116}Tc	^{4}He	^{4}He	^{130}Sb	210.2	13.005

height and width of the barrier and as a result, the barrier penetrability is found to increase. It is observed that the fragments with highest yield are also found to have changed. For the two α-accompanied quaternary fission of ^{244}Cf and ^{246}Cf isotope, the highest yield is found for the fragment combination $^{108}\text{Ru} + ^{4}\text{He} + ^{4}\text{He} + ^{128}\text{Sn}$ and $^{104}\text{Mo} + ^{4}\text{He} + ^{4}\text{He} + ^{134}\text{Te}$, respectively, with the inclusion of deformation. In the case of ^{248}Cf and ^{250}Cf isotopes, the highest yield is found for the fragment combination $^{106}\text{Mo} + ^{4}\text{He} + ^{4}\text{He} + ^{134}\text{Te}$ and $^{110}\text{Mo} + ^{4}\text{He} + ^{4}\text{He} + ^{132}\text{Te}$, respectively. In the case of ^{252}Cf and ^{254}Cf isotopes, the highest yield is found for the fragment combination $^{110}\text{Mo} + ^{4}\text{He} + ^{4}\text{He} + ^{134}\text{Te}$ and $^{112}\text{Mo} + ^{4}\text{He} + ^{4}\text{He} + ^{134}\text{Te}$, respectively. The calculated yield for the quaternary fission of $^{244-254}$Cf isotopes as a function of mass numbers A_1 and A_4, considering both deformation and orientation effects, is plotted in Fig. 8. The Q values and yield for the most favorable fragment combinations for the quaternary fission of $^{244-254}$Cf isotopes are listed in Table I.

Poenaru *et al.*, [17] emphasized the strong shell effect corresponding to the doubly magic heavy fragment ^{132}Sn for the quaternary fission of ^{252}Cf. In our study we observed that the highest yield is obtained for the fragment combinations with ^{134}Sb, ^{134}I, ^{130}In, ^{132}In, and ^{132}Te as one fragment, which is near to ^{132}Sn. This confirms the role of doubly magic nucleus or near doubly magic nucleus in quaternary fission, which supports the conclusion by Poenaru *et al.* [17].

IV. CONCLUSIONS

For the two α-accompanied quaternary fission of $^{244-254}$Cf isotopes, the relative yield is calculated by taking interacting barrier as the sum of Coulomb and proximity potential, with fragments in collinear configuration. In the case of ^{244}Cf and ^{246}Cf, fragment combination $^{102}\text{Tc} + ^{4}\text{He} + ^{4}\text{He} + ^{134}\text{Sb}$ and $^{104}\text{Nb} + ^{4}\text{He} + ^{4}\text{He} + ^{134}\text{I}$ possess highest yield due to the presence of near doubly magic nucleus ^{134}Sb ($Z = 51$, $N = 83$) and ^{134}I ($Z = 53$, $N = 81$), respectively. For ^{248}Cf and ^{250}Cf, the highest yield is obtained for the fragment combination $^{110}\text{Tc} + ^{4}\text{He} + ^{4}\text{He} + ^{130}\text{Sb}$ and $^{110}\text{Rh} + ^{4}\text{He} + ^{4}\text{He} + ^{132}\text{In}$ due to the presence of near proton shell closure $Z = 51$ of ^{130}Sb and near doubly magic nucleus ^{132}In ($Z = 49$, $N = 83$), respectively. For ^{252}Cf and ^{254}Cf isotopes, the fragment combination $^{112}\text{Mo} + ^{4}\text{He} + ^{4}\text{He} + ^{132}\text{Te}$ and $^{114}\text{Tc} + ^{4}\text{He} + ^{4}\text{He} + ^{132}\text{Sb}$, respectively, possess highest yield due to the presence of near doubly magic nucleus ^{132}Te ($Z = 52$, $N = 80$) and ^{132}Sb ($Z = 51$, $N = 81$). It is observed that the highest yield is obtained for the fragment combinations with ^{134}Sb, ^{134}I, ^{130}In, ^{132}In, and ^{132}Te as one fragment, which is near to ^{132}Sn. This confirms the role of doubly magic nucleus in quaternary fission, which supports the conclusion by Poenaru *et al.* [17]. The effect of deformation and orientation is also studied in detail and it has been found that ground-state deformation also plays an important role as that of shell effect in determining the isotopic yield in the two α accompanied quaternary fission of $^{244-254}$Cf isotopes. We hope that our study on isotopic yield in quaternary fission will pave the way for future experiments.

ACKNOWLEDGMENTS

One of the authors (A.C.) would like to thank the Department of Science and Technology (DST), Govt. of India for the financial support under Women Scientist Scheme A (WOS-A) No. SR/WOS-A/PM-26/2016.

[1] V. N. Andreev, Sov. J. Nucl. Phys. **8**, 22 (1969).
[2] A. S. Fomichev, I. David, M. P. Ivanov, and Yu. G. Sobolev, Nucl. Instr. and Meth. A **384**, 519 (1997).
[3] P. Jesinger, Yu. N. Kopatch, M. Mutterer, F. Gonnenwein, A. M. Gagarski, J. v. Kalben, V. Nesvizhevsky, G. A. Petrov, W. H. Trzaska, and H. J. Wollersheim, Eur. Phys. J. A **24**, 379 (2005).
[4] M. Mutterer, Yu. N. Kopatch, P. Jesinger, A. M. Gagarski, F. Gonnenwein, J. v. Kalben, S. G. Khlebuikov, I. Kojouharov, E. Lubkiewics, Z. Mezentseva, V. Nesvizhevsky, G. A. Petrov, H. Schaffner, H. Scharma, D. Schwaln, P. Thirolf, W. H. Trzaska, G. P. Tyurin, and H. J. Wollersheim, Nucl. Phys. A **738**, 122 (2004).

[5] K. P. Santhosh, A. Cyriac, and S. Krishnan, Nucl. Phys. A **949**, 8 (2016).
[6] K. P. Santhosh, A. Cyriac, and S. Krishnan, Indian J. Phys. **92**, 1589 (2018).
[7] J. Blocki, J. Randrup, W. J. Swiatecki, and C. F. Tsang, Ann. Phys. (NY) **105**, 427 (1977).
[8] J. Blocki and W. J. Swiatecki, Ann. Phys. (NY) **132**, 53 (1981).
[9] M. Wang, G. Audi, F. G. Kondev, W. J. Huang, S Naimi, and X. Xu, Chin. Phys. C **41**, 030003 (2017).
[10] P. Möller, A. J. Sierk, T. Ichikawa, and H. Sagawa, At. Data Nucl. Data Tables **109**, 1 (2016).
[11] C. Y. Wong, Phys. Rev. Lett. **31**, 766 (1973).
[12] N. Malhotra and R. K. Gupta, Phys. Rev. C **31**, 1179 (1985).
[13] R. K. Gupta, M. Balasubramaniam, R. Kumar, N. Singh, M. Manhas, and W. Greiner, J. Phys. G: Nucl. Part. Phys. **31**, 631 (2005).
[14] A. J. Baltz and B. F. Bayman, Phys. Rev. C **26**, 1969 (1982).
[15] http://w.w.w.nds.iaea.org/RIPL-2.
[16] P. Moller, J. R. Nix, and K. L. Kratz, At. Data Nucl. Data Tables **66**, 131 (1997).
[17] D. N. Poenaru, R. A. Gherghescu, and W. Greiner, Nucl. Phys. A **747**, 182 (2005).